Combustion and Flame 281 (2025) 114444

Contents lists available at ScienceDirect

Combustion and Flame

journal homepage: www.sciencedirect.com/journal/combustion-and-flame

Propagation of ultra-lean hydrogen/air flames in a Hele-Shaw cell

Linlin Yang [a], Yan Wang [a], Tianhan Zhang [b], Xiaolong Gou [c], Wenjun Kong [b], Zheng Chen [a,*]

[a] SKLTCS, HEDPS, School of Mechanics and Engineering Science, Peking University, Beijing, 100871, China
[b] School of Astronautics, Beihang University, Beijing 102206, China
[c] School of Energy and Power Engineering, Chongqing University, Chongqing 400044, China

ARTICLE INFO

Keywords:
Ultra-lean hydrogen
Flame ball
Flame instability
Flame propagation
Hele-Shaw cell

ABSTRACT

Ultra-lean hydrogen flame is closely related to hydrogen safety. Recently, different types of hydrogen flame have been observed in experiments under ultra-lean conditions. However, the evolution and propagation of ultra-lean hydrogen flames are still not well understood. In this study, 3D simulations considering detailed chemistry and transport models are conducted for ultra-lean premixed hydrogen/air flames propagating in an open Hele-Shaw cell with isothermal walls. It is found that ultra-lean hydrogen flames are very sensitive to equivalence ratio, ϕ. As ϕ decreases from 0.225 to 0.21, different cellular flame regimes, including two-headed branching, two-headed finger and one-headed finger (ball-like flame) are sequentially observed. The cell size shows a decreasing tendency. Isolated ball-like flames and two-headed finger are stable in the ultra-lean mixture. During the flame cell propagation, both heat loss and heat release exhibit oscillatory characteristics since they are correlated with each other. The oscillation frequency is found to increase with ϕ. In order to balance the conductive heat loss to walls, two-headed flames split while isolated ball-like flames shrink, resulting in periodic changes in flame surface area and heat release rate. Moreover, ultra-lean flames are found to be characterized by high local equivalence ratio caused by strong differential diffusion of hydrogen over other species, highlighting the effect of diffusional-thermal instability (DTI) on sustaining the ultra-lean flame. Furthermore, stable ball-like flames and two-headed finger can exist simultaneously. Interestingly, flame instabilities play a stabilizing role in the ultra-lean flames. Darrieus-Landau instability (DLI) contributes to the stabilization of two-headed finger flames with strong mutual interaction between adjacent cells, whereas ball-like flames dominated by DTI tend to move away from each other to gain deficient fuel and drift in a zigzag manner. The present 3D simulations help to understand flame cell propagation and stabilization in ultra-lean hydrogen/air mixture within an open Hele-Shaw cell.

Novelty and Significance Statement

The novelty is that evolution of ultra-lean hydrogen/air flames in an open Hele-Shaw cell was studied and that cellular flame regimes were identified and interpreted. To our best knowledge, 3D simulations for ultra-lean premixed hydrogen/air flames propagating in an open Hele-Shaw cell considering detailed chemistry and transport were conducted for the first time. Different flame regimes were identified and interpreted. The counterintuitive role of hydrodynamic instability in stabilizing ultra-lean flame was discussed.

This study is significant because ultra-lean hydrogen flame relevant to safety is not thoroughly understood due to limitations in previous experiments and simulations. We analyzed the evolution of flame cells and found that heat loss and heat release are correlated with each other and revealed differences in various flame regimes. We also found that hydrodynamic instability stabilizes the two-headed finger flame. This work provides insights to hydrogen flame under near-limit condition.

1. Introduction

As a carbon-free, promising alternative fuel, hydrogen has received increasingly attention recently [1–3]. Compared to traditional

* Corresponding author.
E-mail address: cz@pku.edu.cn (Z. Chen).

https://doi.org/10.1016/j.combustflame.2025.114444
Received 25 February 2025; Received in revised form 24 August 2025; Accepted 29 August 2025
Available online 31 August 2025
0010-2180/© 2025 The Combustion Institute. Published by Elsevier Inc. All rights are reserved, including those for text and data mining, AI training, and similar technologies.

hydrocarbon fuels, hydrogen has a wider flammability range [4,5], which favors fuel-lean combustion with advantage in reducing emission and heat loss [6]. Due to the high diffusivity and reactivity and the small minimum ignition energy of hydrogen, accidentally released hydrogen is prone to be ignited inducing severe explosion [7]. These safety issues pose a serious challenge to industrial applications of hydrogen [1,8]. Even under ultra-lean conditions below the lean flammability limit (i.e., the unstretched planar flame cannot exist), curved hydrogen/air flame can still survive due to the Lewis number effect and propagate as isolated flame cells that are different from ordinary continuous flame front [9, 10]. These isolated flame cells drift in the space and act as ignition kernels as they propagate into mixtures with large equivalence ratio. Therefore, understanding ultra-lean hydrogen/air flame is important for the safe utilization of hydrogen.

There are several studies on ultra-lean premixed hydrogen/air flames. Previous experiments [11,12] in Hele-Shaw chambers showed that ultra-lean hydrogen/air flame can propagate as one-headed finger flame (ball-like flame, flame balls, flame caps, circular flame, or flame ring) or two-head finger flame (double-cell flame, bi-cellular flame). It was proposed that the ultra-lean hydrogen flame is mainly affected by two mechanisms: mass diffusion of hydrogen to increase the local equivalence ratio and heat loss to the wall [11,12]. Besides, the gravity was shown to affect the propagation of ultra-lean hydrogen flame since two-headed cells and one-headed ball-like flames are mainly observed in downwardly and upwardly propagating flames, respectively. More recently, Moskalev et al. [13] has studied the near fuel-lean limit hydrogen/air flames in a horizontal circular Hele-Shaw cell with a fixed width of 5 mm. Under this condition, the effect of gravity was greatly reduced. They found that as the hydrogen concertation increases, the premixed flame changes from discrete cells to quasi-continuous front. The ultra-lean hydrogen/air flame can form ray-like or dendrite-like traces, which are similar to experimental results in [11]. Due to the limited information recorded in experiments, the detailed structure and dynamics were not captured in [11–13]. Therefore, the propagation and evolution for ultra-lean hydrogen flame are still not well understood. Moreover, in previous studies [14,15] the thermoacoustic instability was considered to affect the oscillatory propagation of flame cells in a Hele-Shaw facility. Therefore, the gravity, conductive heat loss, acoustics and their interaction may affect the evolution of ultra-lean hydrogen/air flame, which makes the problem more complicated.

The early numerical study by Grcar [9] have shown that the diffusional-thermal instability (DTI) acts as a stabilizing factor during the ultra-lean flame cells propagation. Numerical simulations [16–19] considered a quasi-2D model and demonstrated that both stable two-headed and one-headed cells can exist without gravity. Through transport budget analysis, it was shown that the ball-like flame is balanced by reaction and diffusion, while for the two-headed finger flame the importance of convection increases [17]. It is also mentioned that the flame evolution can be affected by the initial perturbations on the ignition kernels [17,19]. By changing the ignition perturbation, different regimes can appear at the same equivalence ratio. The recent study [16] found that the formation of stable flame cells is attributed to the symmetry-breaking and reorientiation process after the transient ignition through the postprocessing of flow field. However, these quasi-2D simulations only considered simple transport model and one-step chemistry. Since ultra-lean hydrogen flame is very sensitive to the chemistry and transport model [20], transient simulations considering detailed chemistry and transport should be conducted. Besides, since diffusion plays an important role in ultra-lean hydrogen flame [21, 22], the 3D curvature effect need to be taken into account, necessitating the use of 3D simulations. Moreover, the effect of equivalence ratio was not considered by 3D simulations considering detailed hydrogen chemistry and transport models. Therefore, in literature there is a lack of 3D simulations with detailed chemistry and transport for ultra-lean hydrogen flames with different equivalence ratios.

The isolated ball-like/cap-like flames at ultra-lean condition are of great interest since they are similar to the classic flame balls which were first analyzed by Zel'dovich [23]. In microgravity experiments, Ronney et al. [21,24–26] found that stable flame balls can exist due to radiative heat loss. In the Hele-Shaw cell with cold side walls, the gravity effect can be diminished and conductive heat loss to wall becomes much more important than radiative heat loss. This conductive heat loss is also similar to the role of convection in the counterflow burner [27–29]. In the recent ground-based experiments on hydrogen flame propagation in narrow gaps, Veiga-López et al. [11,12] observed that the ball-like flame has curved and wavy trajectory, which is different from the two-headed flame cell that propagates along a straight line. Recent theoretical studies [30,31] with one-dimensional thermo-diffusive model have shown that the flame cell is a stable solution under heat loss and the size and speed of the flame cell are constant values. It is still not clear why there is such difference in trajectories of one-headed and two-headed flame cells. Besides, the dominant factor for stable two-headed finger flame structure with a straight trace requires further study. This motives us to study the propagation of flame cells and to clarify the differences between these two distinct regimes.

Based on above consideration, this study aims to investigate the evolution and propagation of ultra-lean hydrogen/air flames in an open Hele-Shaw cell. Specifically, 3D simulations on ultra-lean hydrogen flame propagation at different equivalence ratios are conducted by considering detailed chemistry and transport model. The remainder of the paper is structured as follows. Section 2 introduces the details of numerical model used in the simulations. Then in Section 3, the evolution of ultra-lean hydrogen flames and the effect of equivalence ratio are discussed. Finally, in Section 4, the findings of this study are summarized.

2. Numerical model and methods

Here we consider ultra-lean hydrogen flame propagation between two parallel isothermal walls. Due to symmetry, only one-eighth of the physical domain is considered in 3D simulations as shown in Fig. 1. Similar to the experiments in [13], the half-length and half-height of the simulation domain shown in Fig. 1 are $L = 7.5$ cm and $h = 2.5$ mm, respectively. In Fig. 1, three symmetry boundaries are in blue color; while top isothermal, no-slip wall with fixed temperature of $T_W = 300$ K is in grey. Fig. 1 also shows that outlet boundaries are enforced. Therefore, the effect of acoustic wave on flame evolution is not considered here.

The computational domain is initially filled with static, premixed hydrogen/air mixture at $T_0 = 300$ K and $P_0 = 1$ atm. The mixture composition is determined by the equivalent ratio, ϕ, to be specified for different cases. To initiate flame propagation, we set a hot spot with temperature of $T_H = 2000$ K and radius of $R_H = 5$ mm at the origin. Note that large hot spot size is used since it is difficult to ignite ultra-lean hydrogen/air [32]. Besides, the hot spot size is close to the ignition kernel size observed in experiments [13]. To promote flame instability and flame splitting, we enforce the following perturbation on the hot

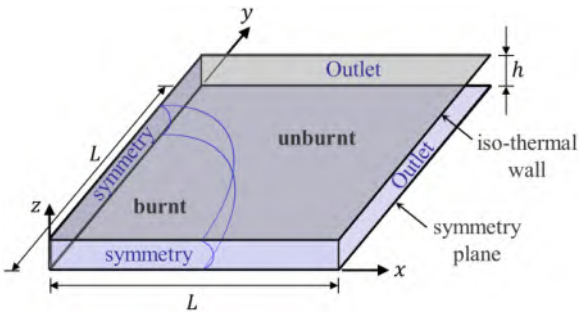

Fig. 1. Schematic of the 3D computational configuration. Due to symmetry, only 1/8 of the Hele-Shaw cell is shown.

spot surface:

$$r = R_H + A\sin(4n\theta) \quad (1)$$

where $A = 0.1$ mm is the amplitude of the initial perturbation, n the wavenumber, and θ the polar angle which is in the range of $[0, \pi/2]$ for the computational domain shown in Fig. 1. Different equivalence ratios are considered in the simulations. We choose $n = 3.5$ unless otherwise specified. For $\phi = 0.210$, additional cases with $n = 1.5$ and $n = 2.5$ are considered to study the effects of initial perturbation of the hot spot surface. In this study, a specific form of the ignition kernel perturbation is employed to excite the flame regimes observed in previous experiments. In future works, it will be interesting to assess the effects of initial perturbation (e.g., a fully random perturbation) on the transient evolution of flame cells. For each equivalence ratio, the corresponding hydrogen molar fraction, X_{H2}, adiabatic flame temperature, T_{ad}, and hydrogen Lewis number *Le* are listed in Table 1. It is seen that the adiabatic temperature based on total enthalpy conservation is <1000 K, which is around the crossover temperature of hydrogen (below which chain-branching reactions cannot sustain) [10]. Therefore, for such low equivalence ratio the unstretched planar flame cannot exist. Note that for all the equivalence ratios considered here, the Lewis is small but very close for all cases. This indicates that there is strong differential diffusion in all cases and that the different flame behaviors for different equivalence ratios are not caused by the difference in Lewis number, which was mentioned by Yáñez Escanciano et al. [12].

The transient flame propagation process is simulated using the open-source code, PeleLMeX [33], which solves the Naiver-Stokes equations for a multi-component reactive flow in the Low-Mach number limit. Acoustic waves are filtered out and thereby the flame propagation is not affected by thermoacoustic instability. The details on governing equations, numerical methods and code validation for PeleLMeX can be found in [33] and thereby are not repeated here. The detailed kinetic model for hydrogen oxidation from FFCM-1[34] and the mixture-averaged transport model are used in all simulations. As a first step to understand 3D ultra-lean hydrogen flames in a Hele-Shaw cell, in simulations here the gravity and radiative heat loss are not considered, which need to be explored in future studies.

To accurately and efficiently simulate the transient flame propagation, we use adaptive mesh refinement with the finest grid size of $\Delta x = 80$ μm. The reaction zone is fully covered by the finest grids and well resolved. Grid convergence is achieved and demonstrated in the Supplementary Material. It is noted that symmetry boundary conditions may influence various instabilities [35] by altering spatial scales. To validate their use in this study, additional simulations are conducted without applying symmetry boundary conditions in the xy-plane and z-direction, respectively. These results (provided in the Supplementary Material) demonstrate that symmetry boundary conditions do not affect the evolution of isolated flame cells.

3. Results and discussion

3.1. Flame cell evolution and different regimes

Fig. 2 shows the evolution of two-headed branching flame cell for $\phi = 0.225$. The flame cell is represented by the isosurface of temperature at 1000 K. To distinguish different instants, the contour of heat release rate (HRR) and vorticity is presented ~~alternatively~~ in Fig. 2. The smooth and continuous flame front quickly splits into two large cells after ignition. As they propagate outwardly, flame cell expands and splits again, forming four smaller cells. This stage with four cells also appears in other cases with different ϕ. Therefore, flame evolution in the early stage is similar, which might be affected by ignition and initial perturbation imposed on the initial hot spot. The ignition effect quickly decays as flame propagates outwardly.

Table 1
The hydrogen molar fraction X_{H2}, adiabatic flame temperature T_{ad}, and hydrogen Lewis number *Le* for mixtures with different equivalence ratios ϕ.

ϕ	0.225	0.220	0.215	0.210
X_{H2}	8.63 %	8.46 %	8.28 %	8.10 %
T_{ad} (K)	988	976	959	947
Le	0.337	0.335	0.335	0.334

In the late stage, it is interesting that two adjacent flame cells always propagate outwardly in pair and they do not move away from each other. This indicates that there is strong mutual interaction between these two adjacent flame cells. As shown in Fig. 2, large HRR mainly appears on the head of the flame cells, while much lower HRR appears on the tail and top side of the flame cell. The top side of the flame cell suffers strong heat loss to the isothermal wall. Due to mutual interaction, HRR is enhanced on the cell head. Owing to the balance between heat and mass diffusion, these two flame cells do not merge with each other. This two-headed finger flame is similar to the structure of flame finger observed in thermo-diffusively unstable flames [36,37], indicating the significant influence of thermal-diffusively instability on the ultra-lean hydrogen mixture.

In the previous study on the mutual interaction among flame balls by Ronney et al. [26], it is mentioned that when two adjacent flame balls are close to each other, their mutual interaction increases the temperature in the region between them and thereby results in relatively large HRR therein. Therefore, these two flame balls tend to move towards each other. On the other hand, due to the depletion of fuel, these two flame balls tend to drift apart to gain more fuel. The net effect is mutual repulsion between flame balls. Obviously, this mechanism is not applicable for the two-headed finger flame in this study which propagates straightly in a stable structure. This indicates that processes other than diffusion and heat loss must be considered in the propagation of the two-headed finger flame. The mechanism of stabilizing two-headed finger flame will be discussed later.

Due to cell expansion, Fig. 2 shows that cyclical cell splitting happens on the tails of the two-headed cell. The small flame pockets move towards the burned gas immediately after the cell splitting. They quickly extinguish and disappear due to the wall heat loss and the lack of hydrogen in the burned gas. However, at late stage separated flame pockets can last for relatively long period since the amount of unburned hydrogen increase with flame radius. These isolated flame pockets expand and then propagate towards the unburned gas.

Fig. 2(b) shows that strong vorticity appears on the cell top, which is induced by the no-slip wall. Therefore, the flow in the *z*-direction is complicated and affects the flame cell evolution, which cannot be captured by previous quasi-2D simulations. This also highlights the 3D nature of flame cell propagation in the narrow Hele-Shaw cell.

To show the details on the cell splitting process, a representing splitting process for $\phi = 0.225$ is shown in Fig. 3. In Fig. 3(a), the temperature (which also reflects the flame intensity) on the head of near-diagonal cells is relatively uniform due to small flame size, while for the near-axis cells the temperature in the middle part is relatively low. Since each branch of the two-headed flame cell has a trend to expand outwardly, the flame cells are elongated as they propagate, resulting in a large cell size for near-diagonal cells or a long tail for near-axis cells, as shown in Fig. 3(a) and (b). It is noted that for the elongated flame cell, the curvature in the middle part is reduced. The flame intensity reduces due to negative stretch rate there, resulting a small cusp in the middle of flame cell, as shown in Fig. 3(b). Once the cusp is formed, the local negative stretch further suppresses chemical reaction near the cusp, causing a deeper cusp shown in Fig. 3(c). Consequently, cell splitting starts to occur near the deep cusp. Finally, Fig. 3(d) shows that isolated flame pockets form. Due to the heat loss to wall and lack of hydrogen, the separated flame pocket cannot sustain for long period of time and it quickly extinguishes. Nevertheless, the cell splitting reduces the flame cell size and thereby increases the curvature of the flame cell. This helps to improve the flame intensity and HRR since the Lewis

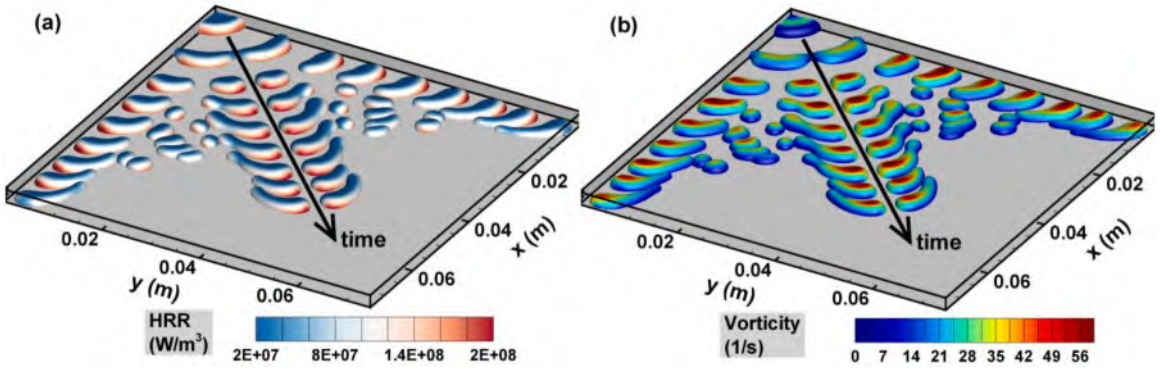

Fig. 2. Temporal evolution of the temperature isosurface colored by (a) heat release rate (HRR) and (b) vorticity for $\phi = 0.225$. The animation is in the Supplementary Material. The corresponding instants are $t = 0.010$ s, 0.058 s, 0.110 s, 0.154 s, 0.198 s, 0.241 s, 0.284 s, 0.325 s, and 0.367 s.

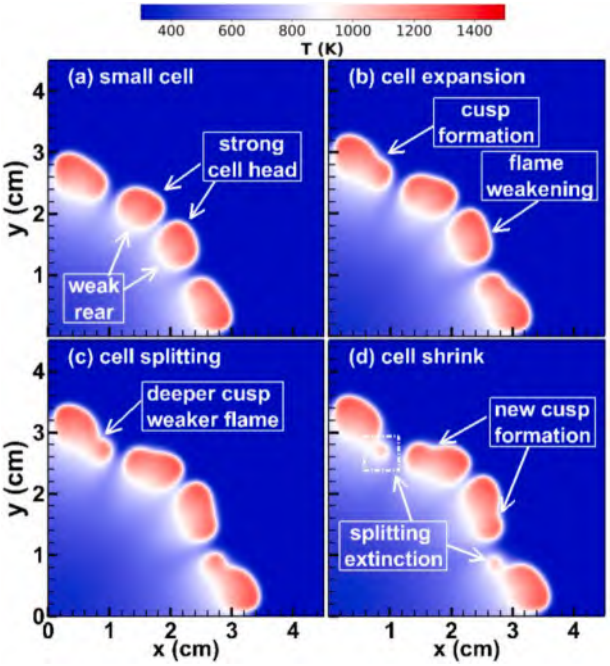

Fig. 3. Evolution of the temperature contour on the symmetry plane, $z = 0$, during the cell splitting process for $\phi = 0.225$: (a) $t = 0.12$ s, (b) $t = 0.134$ s, (c) $t = 0.142$ s and (d) $t = 0.15$ s. The animation is provided in the Supplementary Material.

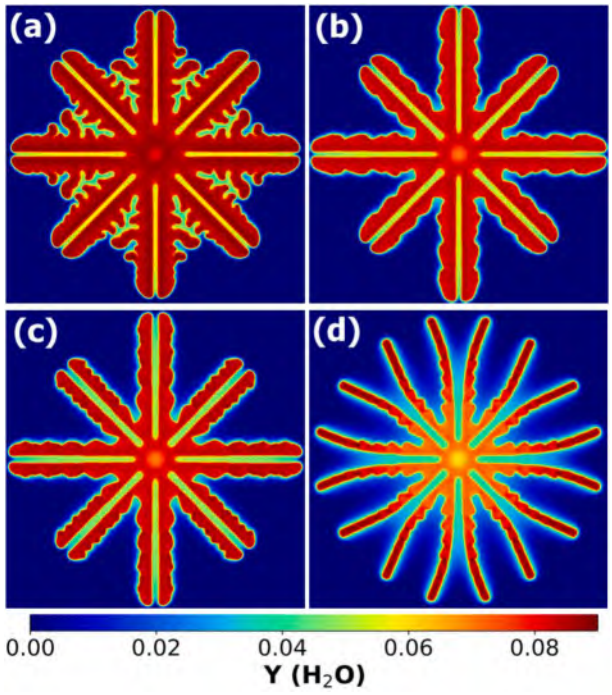

Fig. 4. The recorded history of the maximum water vapor mass fraction (Y (H_2O)) on the symmetry plane, $z = 0$, for (a) $\phi = 0.225$, (b) $\phi = 0.220$, (c) $\phi = 0.215$ (d) $\phi = 0.210$. The animation is provided in the Supplementary Material.

number is very small. Therefore, the two-headed cell can increase its intensity through cell splitting on its tails and thereby sustain in the ultra-lean hydrogen/air mixture. To maintain its size/curvature, cell splitting happens periodically during its propagation (see Fig. 2). It is worth noting that the flame cell branches are asymmetric in Fig. 3, differing from the splitting process of classical flame balls in [38,39]. This asymmetry originates from the non-uniform curvature distribution on the two-headed flame finger front. Flame branching tends to occur on the tail of the flame cell where curvature and chemical heat release are lower than on the head. This contrasts with the splitting process of classical flame balls, which exhibit spherical symmetry and commonly display symmetric branching.

Apart from the two-headed branching flame regime discussed above, other flame regimes including two-headed finger and one-headed finger are observed for other equivalence ratios. This is similar to results from experiments [13]. To compare with the condensed water streaks recorded in experiments [11,13], Fig. 4 shows the recorded history of maximum water vapor mass fraction, Y(H_2O), for different values of ϕ.

For $\phi = 0.225$, Fig. 4(a) shows that the flame cell propagation forms a two-headed branching trajectory, consisting of two trunks with small bifurcated branches along each side, like fern and leaves. Obviously, the fern is caused by the two-headed cell while the leaves correspond to small separated flame pockets. As explained before, in the late stage the bifurcated flame pockets can exist for relatively long time and thereby form relatively large leaves on the trajectory.

For $\phi = 0.220$ and $\phi = 0.215$, Fig. 4(b) and (c) show that their trajectories are similar and both can be categorized into the two-headed finger regime. It is seen that both sides of each straight trajectory are wavy but there is no bifurcated cell. This phenomenon is slightly different from the experiment observation [11,12], in which the trace of condensed water is straight with nearly constant width. In fact, close observation of the supplementary material for Ref. [11] indicates that the two-headed cell exhibits weak variation in its width, which is consistent with simulation results reported here. Besides, in experiments [11] there might be weak cell splitting occurring on the tail. However, flame extinction happens quickly, making the wavy trajectory not

obvious.

When the equivalence ratio is further reduced to $\phi = 0.210$, Fig. 4(d) shows a new flame regime with one-headed finger trajectory. The ball-like flame trajectory is shown to be characterized by two distinguishing stages: the first stage exhibits a narrow trace with wavy structure on its sides, while in the second stage the trajectory is quite smooth. Interestingly, Fig. 4(d) shows that as the ball-like flames propagate outwardly, they tend to distribute uniformly on a circle. This is reasonable because such uniform distribution helps to consume as much hydrogen as possible. The detailed ball-like flame evolution will be discussed in Section 3. 4.

3.2. Analysis on flame cell propagation

The animations for the flame cell propagation at different equivalence ratios are provided in the Supplementary Material. To quantify the flame cell propagation, in Fig. 5 we plot the temporal evolution of the leading points and its propagation speed for a flame cell near the x-axis. Note that the leading point is defined as the farthest point from the origin on the isosurface with $c = (T\text{-}T_0)/(T_{max}\text{-}T_0) = 0.8$. As expected, the leading point for higher ϕ moves faster along the x direction due to the stronger reactivity. Though the selected leading points are closed to the x-axis and have small displacement in the y direction, the drifting distance along the y direction is the largest for ball-like flame with the smallest ϕ. This can also be observed in Fig. 4 that the trajectories for ball-like flames are significantly curved. Fig. 5(b) also shows that the oscillation along y direction becomes stronger for lower ϕ. This simulation results agrees well with the experimental observation that ball-like flames tend to drift in a zigzag manner in the early stage of propagation [11,12]. Moreover, Fig. 5(c) shows that the speed of the leading point increases monotonically with ϕ. This is consistent with results in Fig. 5(a) since the propagation in the x direction dominates for the selected flame cell near the x-axis. Besides, Fig. 5(c) shows that there is obvious oscillation in the propagation speed. It is found that the propagation speed reaches its local minimum after cell splitting or shrinking, demonstrating the oscillatory feature is caused by the unsteady cell evolution.

To quantify the overall combustion process, we calculate the integral heat release rate, iHRR, within the whole domain and the conductive heat loss to the cold wall, Q_W. The results are shown in Fig. 6(a) and (b). As expected, it is seen that the higher the ϕ, the larger the iHRR and Q_W. Meanwhile, oscillation is observed for both iHRR and Q_W and the frequency is shown to increase slightly with ϕ. This is because the cell evolution is more active at larger ϕ. The characteristic frequency f can be roughly estimated by the rate between propagation speed u shown in Fig. 5(c) and the separated flame pocket size d. It is noticed that d is almost the same for the narrow range of ϕ considered here while there is obvious increase of u with ϕ according to Fig. 5(c). Consequently, the frequency of the oscillation induced by cell splitting increases with ϕ.

Figs. 6(a) and (b) also show that there is a phase lag in Q_W compared to iHRR for $\phi \leq 0.220$. When the iHRR reaches its peak, Q_W increases until it reaches the local maximum. This indicates that the chemical heat release and conductive heat loss are correlated with and restricted to each other. As shown in the inserts in Fig. 6(a), the iHRR reaches local maximum/minimum value when flame cells are large/small. Peak Q_W appears at the moment immediately before cell splitting happens (see the inserts in Fig. 6b). However, the minimum value of Q_W is reached when the flame cell starts to expand in size.

Fig. 6(c) and (d) plot the total flame surface area, A_f, and averaged heat release rate, q, which is defined as q = iHRR/A_f. Here the flame surface is defined as the isosurface with the progress variable of $c = 0.8$. Note that A_f and q approximately quantify the flame cell size and the flame intensity, respectively. Comparison between Fig. 6(c) and (a) indicates that the evolution of A_f is almost synchronized with the iHRR. Therefore, the increase in iHRR is mainly caused by the growth of the flame surface area, which is caused by the expansion of flame cells. On the contrary, the evolution of q is almost in the opposite trend compared to A_f and iHRR. This can be explained as follows. After splitting for two-

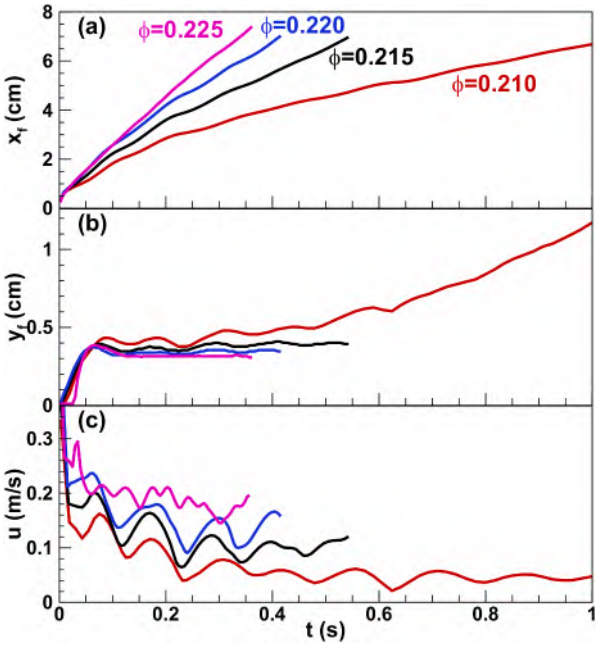

Fig. 5. Change of the leading point position (x_f, y_f) and corresponding propagation speed u with time for different equivalence ratios.

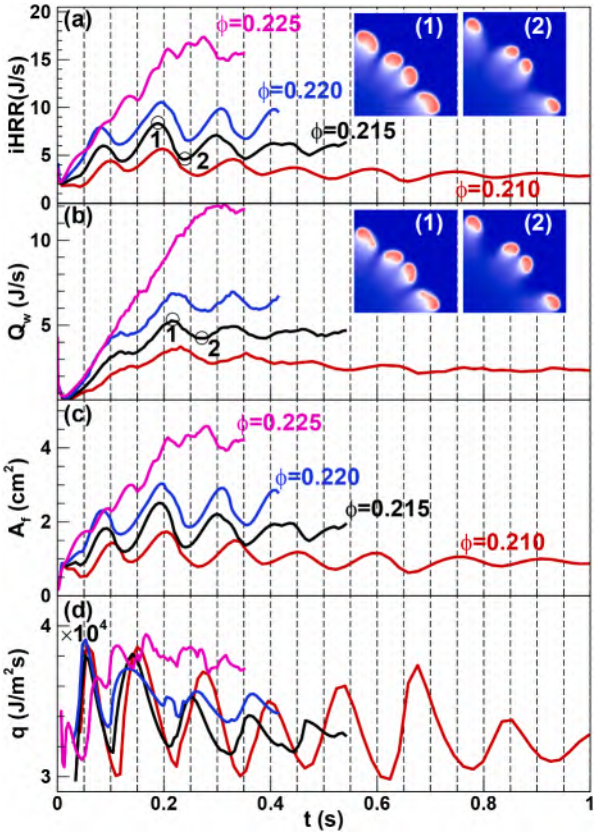

Fig. 6. Evolution of (a) integral heat release rate, iHRR, (b) conductive heat loss on the wall, Q_W, (c) total flame surface area, A_f, and (d) averaged heat release rate, q, for different equivalence ratios. The inserts are temperature contours on the symmetry plane at $z = 0$ for two instants marked by circle 1 and 2 in Figs. (a) and (b).

headed cells, the cell continuously shrinks until iHRR and A_f reaches their local minima. During this process, A_f decreases while q increases gradually, indicating the enhancement of local chemical reaction. Due to weak flame caused by decreasing iHRR and flame surface area A_f, the Q_W also decreases during the shrinking of flame cell. At certain instant, flame cell no longer shrinks, and both iHRR and A_f begin to increase. Then Q_W reaches its minimum value and begins to increase until the next splitting happens. This process occurs periodically, causing the oscillatory evolution shown in Fig. 6. In summary, the correlation and competition between the chemical heat release and wall heat loss dominate the evolution of ultra-lean flame cells and leads to the oscillatory features in iHRR, Q_W, cell speed and size.

On the other hand, it is noticed from Fig. 6 that the instant when Q_W reaches its peak value is slightly behind that for A_f. This indicates that flame cells tend to reduce heat loss by reducing their surface area or size. Specifically, for two-headed cells the splitting on the tail helps to reduce heat loss, while for ball-like flames the shrinking helps to reduce the heat loss.

According to the trajectory width shown in Fig. 4 and the opposite trends for A_f and q respectively shown in Figs. 6(c) and (d), it can be concluded that the cell size is an important parameter to characterize the ultra-lean hydrogen/air flame. To explain this, we plot the HRR in terms of the mean curvature κ and local equivalence ratio ϕ_c in Fig. 7. This 2D histogram shows the distribution of average HRR as a function of mean curvature and local equivalence ratio. The mean curvature κ is the arithmetic average of the two principal curvatures at a point on the surface and it is calculated based on the isocontour lines of $Y(H_2O)$, i.e.,

$$\kappa = \nabla\cdot\vec{\boldsymbol{n}}/2 \ with \ \vec{\boldsymbol{n}} = -\nabla Y(H_2O)/|\nabla Y(H_2O)| \tag{2}$$

where $\vec{\boldsymbol{n}}$ is the unit normal vector of the flame surface pointing toward the unburned gas. To quantify the effects of differential diffusion of hydrogen on the mixture composition, we calculate the local equivalence ratio ϕ_c based on the element molar fraction of hydrogen and oxygen, X_H and X_O:

$$\phi_c = X_H/(2X_O) \tag{3}$$

For $\phi = 0.225$, Fig. 7(a) shows that the HRR is non-negligible for a wide range of κ and ϕ_c. When ϕ_c equals the overall equivalence ratio $\phi = 0.225$, the HRR is almost negligible. The HRR peaks around $\phi_c \approx 0.3$, indicating that the differential diffusion of hydrogen can greatly increase the local equivalence ratio and thereby is important for the two-headed branching regime. In fact, for ultra-lean hydrogen, a slight increase in equivalence ratio can greatly improve the burning rate [10]. By contrast, for ball-like flames in Fig. 7(b) the large values of HRR are restricted to a relatively narrow region with large κ and ϕ_c, highlighting that chemical heat release occurs only in regions with both high curvature and high local equivalence ratio. Besides, the peak HRR occurs at $\phi_c \approx 0.38$ for $\phi = 0.210$, which is much higher that $\phi_c \approx 0.3$ for $\phi = 0.225$. This indicates that stronger differential diffusion of hydrogen happens to ball-like flames. This is reasonable since the smaller ϕ leads to reduction in mixture reactivity, necessitating stronger differential diffusion of hydrogen to increases the local equivalence ratio ϕ_c.

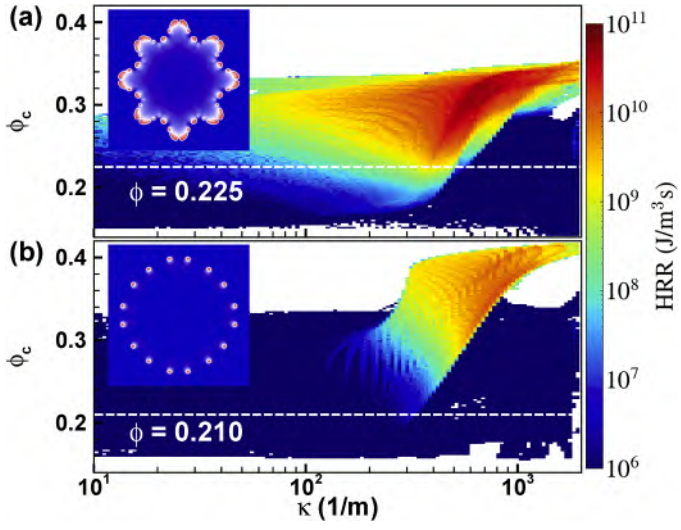

Fig. 7. The 2D histogram of the HRR as a function of the mean curvature κ and local equivalence ratio ϕ_c at nearly the same flame radius for (a) $\phi = 0.225$ at $t = 0.304$ s and (b) $\phi = 0.210$ at $t = 0.871$ s. The dashed white lines represent the global equivalence ratio, ϕ. The inserts are the corresponding temperature contours on the symmetry plane at $z = 0$.

It is noteworthy that for different equivalence ratios considered here, their Lewis numbers are close (see Table 1), but the flame regimes are quite different (see Fig. 4). Therefore, the flame regime is not determined by the Lewis number. Nevertheless, the differential diffusion quantified by Lewis number is crucial for ultra-lean hydrogen flame [12]. The decreasing trend in cell size with a decreasing equivalence ratio ϕ can be interpreted by the Lewis number effect. Due to small Lewis number, the differential diffusion facilitates the ultra-lean flame with large curvature. As ϕ decreases, the mixture reactivity and heat release decrease and thereby the relative importance of heat loss increases. Therefore, the chemical reaction is restricted to a narrow region with very large mean curvature as well as relatively high local equivalence ratio. Since the Lewis number of ultra-lean mixture is close (see Table 1), larger curvature of flame surface is required for smaller ϕ. For small ϕ, the flame curvature distribution tends to be more concentrated, which is the feature of ball-like flames. This also explains the experimental results that as the heat loss effect further increasing by decreasing the gap distance, flame cells appear in the regimes of isolated ball-like flames [11].

3.3. Effect of hydrodynamic instability on stable two-headed finger flame

Although changing the equivalence ratio can lead to different flame regimes, it is found that the perturbation on the ignition hot spot can also affect the flame evolution regimes. In this section, we do not aim to comprehensively explore the impact of initial perturbations on flame evolution. A slightly different initialization from that used in previous sections is employed to obtain both one-headed and two-headed finger flames under the same equivalence ratio. This approach can remove the influence of equivalence ratio on flame regimes and effectively highlights the differences between the two flame regimes.

Fig. 8 shows the recorded history of the maximum water vapor mass fraction on the symmetry plane for $\phi = 0.210$ and $n = 2.5$. The flame propagation exhibits a hybrid regime including both the one-headed finger and two-headed finger flame cells. Different regimes in the near-diagonal and near-axis directions are reasonable since the ignition kernel is not equivalent in these two directions. Note that in Fig. 4(d) the flame regime is one-headed finger for $\phi = 0.210$ and $n = 3.5$. Therefore, the ultra-lean flame is also sensitive to the ignition process. Equivalence ratio ϕ can affect the flame regimes, but it is not the only factor that distinguishes these two stable regimes. This is also mentioned in the recent study [19]. It is also noted that the formation of these two stable regimes can be reproduced using different initial perturbations and without applying symmetry boundary conditions, indicating that these regimes are not numerical artefacts. Previous experiments and simulations [11,19] have also demonstrated the existence of such flame regimes.

As shown in Fig. 8, the two-headed finger flame propagates faster than the ball-like flames (one-headed finger flame). To quantify the propagation speed or drifting speed of flame cells, the evolution of drifting speed for two-headed finger and ball-like flames is plotted in Fig. 9. In the early stage ($t < 0.3$ s), the flame propagation speed is relatively large since it is affected by the transient ignition process. Then the drifting speed exhibits an oscillatory feature, which is caused by the

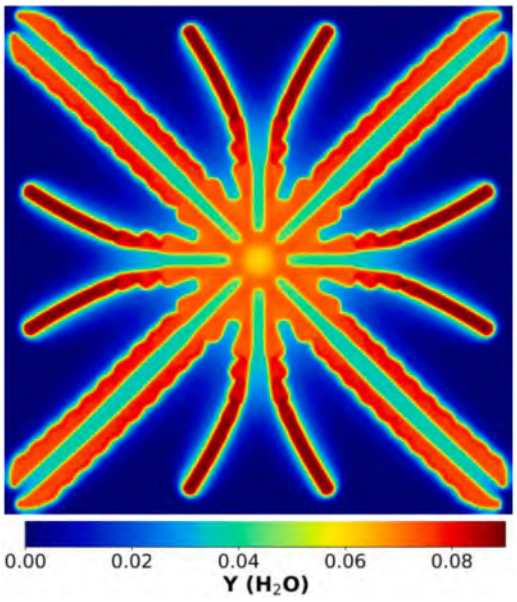

Fig. 8. The recorded history of the maximum water vapor mass fraction (Y (H_2O)) on the symmetry plane, $z = 0$ for ϕ=0.210 and $n = 2.5$.

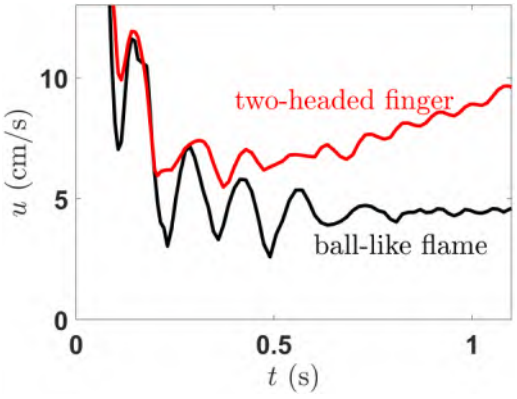

Fig. 9. Evolution of drifting speed of the ball-like flame (near axis) and the two-headed finger (near diagonal) flame cells for $\phi = 0.210$ and $n = 2.5$.

competition between wall heat loss and flame stretch effect. In the late stage of flame evolution ($t > 0.5$ s), the amplitude of drifting speed oscillation decreases. The drifting speed of ball-like flames approaches a constant value, while that of two-headed finger increases slightly. This is because ball-like flames reach their steady state earlier than the two-headed finger as the flame cells drift away from each other. In Fig. 8, wavy structure disappears on the traces of ball-like flames, demonstrating the steady state is reached. At the end of flame cells propagation, the propagation speed of two-headed finger is approximately twice as that of the ball-like flames. This result agrees with the previous study [19]. Note that the slight increase in drifting speed of two-headed finger flame cells is reasonable since more fuels can be supplied to the flame cells as they drift apart.

The evolution of the maximum of temperature T_{max} and heat release rate HRR_{max} near the ball-like flame and the two-headed finger is shown in Fig. 10. After ignition, T_{max} and HRR_{max} decrease gradually. For the near-axis ball-like flames, T_{max} and HRR_{max} reach constant values as ball-like flames are in steady state. However, slight increase in T_{max} and HRR_{max} indicates that the two-headed finger becomes stronger as it propagates outwardly. This is consistent with the trend of drifting speed which increases in the late stage for the two-headed finger flame cell. In the late stage of flame cell propagation, T_{max} for ball-like flames and

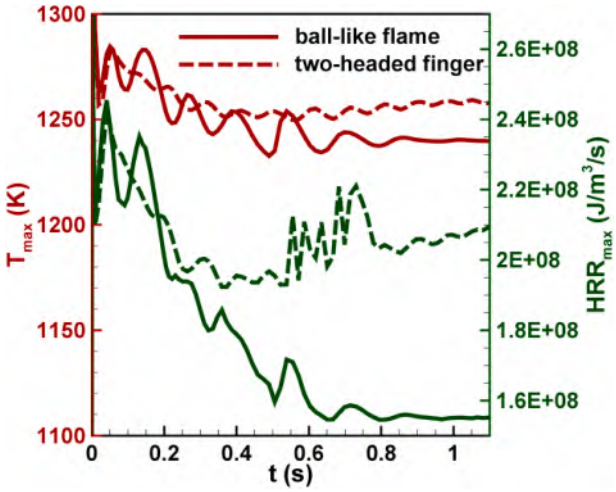

Fig. 10. Evolution of the maximum of temperature T_{max} and heat release rate HRR_{max} near the ball-like flame and the two-headed finger flame.

two-headed finger are around 1230 K and 1250 K, respectively. This shows that chemical reactions near the two-headed finger is slightly more intense that those near the ball-like flames. The T_{max} is much higher than the adiabatic temperature after complete reaction, demonstrating that DTI is vital for the sustainment of ultra-lean flames.

It is interesting to mention that the propagation of two-headed finger structure in both two-headed finger and the two-headed branching regimes forms a straight trace. On the contrary, the propagation of ball-like flames often leaves a curved trace due to its zigzag motion. Therefore, there exists a stabilizing mechanism for the two-headed finger structure. Both regimes can form at the same equivalence ratio shown in Fig. 8, providing a suitable configuration to clarify the stabilizing mechanism.

It is found that the hydrodynamic instability (DLI) significantly affects the propagation of two-headed finger flame. Note that for the ultra-lean hydrogen considered in this study, DTI is definitely an important factor influencing flame cell sustainment and propagation. Nevertheless, DLI also plays a role in affecting flame propagation through stabilizing effect and its synergistic interaction with DTI.

To explain the role of DLI, streamlines superimposed on the vorticity magnitude contour near the symmetry plane ($z = 0$) are shown in Fig. 11. As mentioned in [40–43], although both DTI and DLI can produce wrinkles on the flame front, the vorticity production is a defining feature for DLI. Therefore, the vorticity near the flame front can be used as an indicator of DLI. It is seen from Fig. 11(a) that the magnitude of vorticity near the ball-like flames are much smaller than that near the two-headed finger flame. The streamlines divergence phenomenon in Fig. 11 clearly shows stronger flame-flow interaction near the two-headed finger flame, demonstrating the effect of DLI during flame cell propagation. Moreover, for the two-headed finger, the magnitude of vorticity near the two middle branches forming the cusp is larger, indicating that mutual interaction between two flame branches can enhance the flame-flow interaction as well as the DLI instability. This is reasonable since the two adjacent cells of the two-headed finger flame form a large flame segment with a deep cusp, which strongly affects the flow field near the flame cell. Note that these two flame cells have a tendency to drift apart to gain more fuel. The formation of strong vortex near the cusp tends to merge the two adjacent cells and prevent their separation. Therefore, DLI helps to form a stable two-headed finger structure. For the ball-like flames, the cusp structure cannot form. The flame-flow interaction is weak and the streamlines near ball-like flames are different from those near the two-headed finger flame, as shown in Fig. 11. Therefore, ball-like flames are less affected by DLI during the propagation.

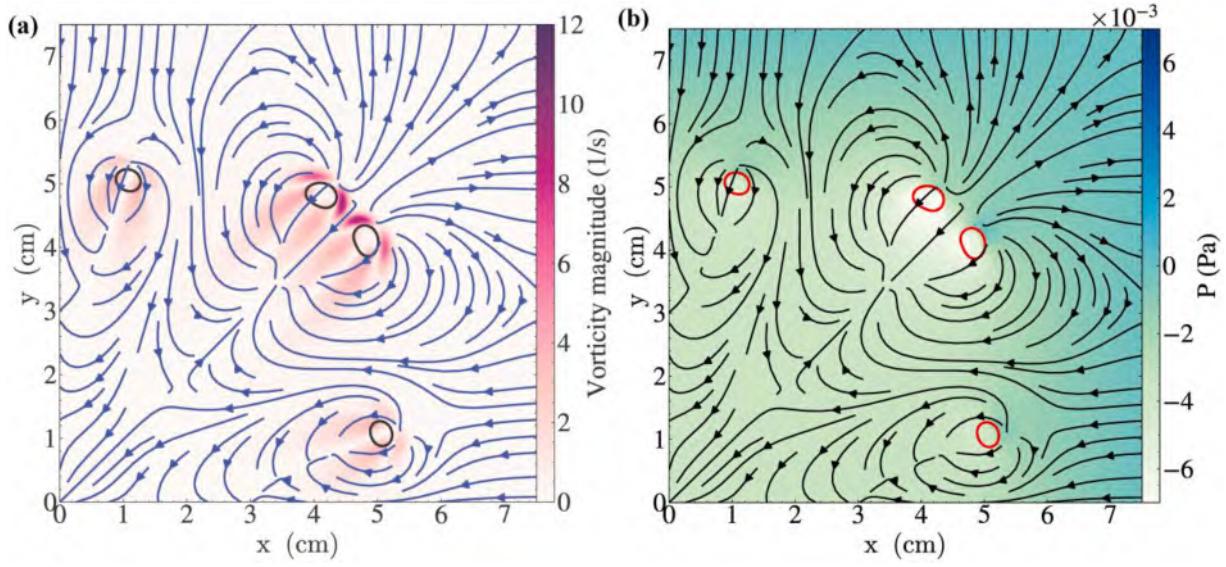

Fig. 11. Streamlines superimposed on the contours of (a) vorticity and (b) hydrodynamic pressure near the symmetry plane $z = 0$ at $t = 0.73$ s for $\phi = 0.210$ and $n = 2.5$. Circles denote the isocontour of $T = 1000$ K.

Fig. 12 shows the temporal evolution of maximum vorticity near ball-like flames and two-headed finger flame. It is seen that in the late stage of flame propagation, the vorticity near the two-headed finger flame is consistently larger. This implies that DLI for the two-headed finger flame will be more pronounced than that for ball-like flames when they finally reach the steady states. Note that DLI may have synergetic interaction with DTI, favoring the propagation of two-headed finger flame, as the directions of streamlines ahead of the flame cells are different (see in Fig. 11(a)). Similar phenomena are explained in the previous studies [36] for fuel-lean hydrogen/air flame. This also explains why the drifting speed of the two-headed finger flame is faster than that of the ball-like flames, as shown in Fig. 9.

It is generally accepted that for the fuel-lean hydrogen/air flame, the DTI dominates over DLI. The formation of flame finger is purely attributed to DTI [36]. However, the present results show that DLI may be also important for ultra-lean flames as it helps to stabilize the two-headed finger flame. Note that the DTI, rather than the DLI, is the primary mechanism responsible for the formation of isolated flame cells under ultra-lean conditions. The formation of two-headed finger flames does not necessarily require the presence of DLI, as demonstrated in a previous study [44], where the double-cell structure was captured using a purely diffusive-thermal model without accounting for flow effects. However, hydrodynamic instability contributes to the stabilization of two-headed finger flames by modifying the local flow field. Flow acceleration near the center of two-headed finger flames forms a low-pressure region, as shown in Fig. 11(b). This pressure gradient tends to draw the two branches closer together, promoting a more stable structure. This is also supported by the simulation [16] that considers thermal expansion effects, where a higher expansion ratio favors the evolution of two-headed finger flame cells. It is also noteworthy that the enhancement of DLI is not through promoting gas expansion across the flame front, as the expansion ratio (see T_{max} in Fig. 10) is almost the same for ball-like flames and the two-headed finger flame. In fact, DLI is enhanced by forming larger flame segments with a cusp through mutual interaction. The isolated ball-like flames cannot form a cusp and thereby suppress the development of DLI.

In short, both two-headed finger flame and ball-like flames can appear simultaneously at the same equivalence ratio. The flame propagation regime is affected by both equivalence ratio and the initial ignition kernels. The two-headed finger flame formed through mutual interaction between its two cells acts as a cusp-like structure and thereby induces stronger DLI. Therefore, the DLI can stabilize the two-headed finger flame and helps to form a straight trace. Synergistic interaction between DTI and DLI leads to higher drifting speed of two-headed finger flame.

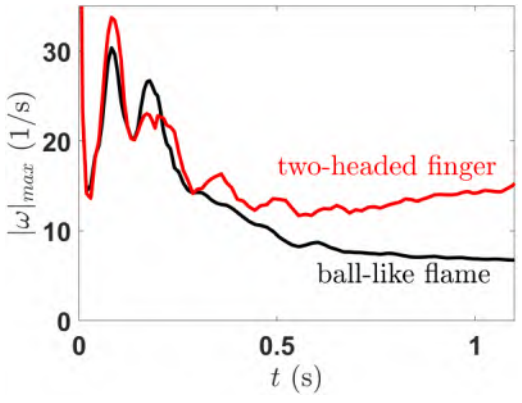

Fig. 12. Evolution of maximum vorticity near ball-like flames and two-headed finger flame.

3.4. Evolution of ball-like flames

One difference between two-headed finger and one-headed finger is that the trajectory for ball-like flame is curved due to the zigzag motion. This phenomenon was mentioned by Kagan and Sivashinsky [45]. Recent experiments [11] clearly showed that after ignition, ball-like flames move alternatively toward the left and right sides. However, in the late stage the ball-like flame trajectory is almost straight. Fig. 13 shows the zigzag propagation of the ball-like flames with two initial perturbations of $n = 3.5$ and $n = 1.5$. The zigzag propagation is caused by the weak splitting of ball-like flames. When the elongated flame cell evolves into a spherical ball through similar but weak splitting mechanism in Fig. 3, the ball-like flame propagation direction changes. This is because only part of the cell exists after the elongated flame cell evolves to ball-like flame.

Fig. 13 also shows that the ball-like flame evolution in the late stage is quite different from two-headed flame cell shown in Fig. 2. First, two adjacent cells near the diagonal move away from each other quickly.

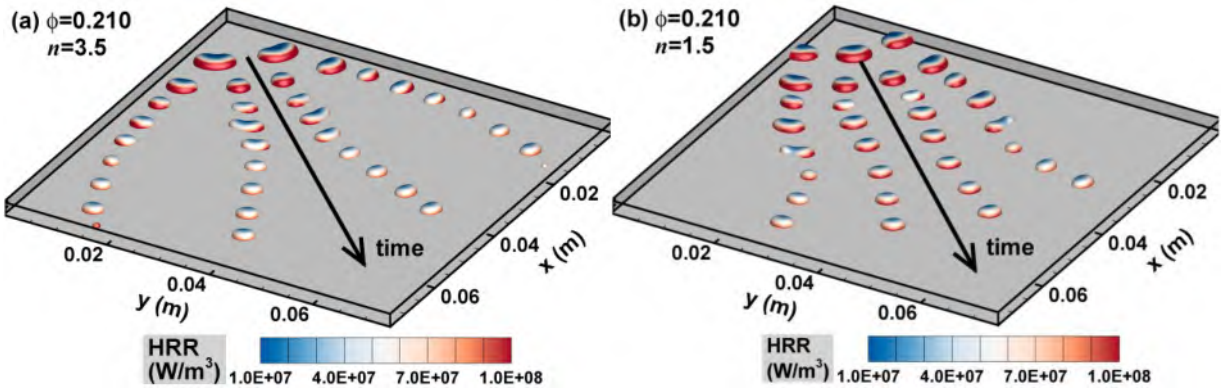

Fig. 13. Temporal evolution of the temperature isosurface colored by heat release rate (HRR) during ball-like flame propagation in the H_2/air mixture with ϕ = 0.210 for (a) n = 3.5 and (b) n = 1.5. The animation is provided in the Supplementary Material.

This indicates that there exists mutual interaction between these two ball-like flames. Consequently, the distance between two ball-like flames increases as they propagate outwardly. This is similar to the mutual propulsion in microgravity experiments in [26]. Second, there is no obvious cell splitting. Though elongated ball-like flames can be observed in the early stage in Fig. 13, cell splitting doesn't happen in the late stage. Third, the flame cell size is smaller than that for ϕ = 0.225. This is because chemical reaction occurs only in regions with very large flame curvature, which is explained in Section 3.2.

Fig. 14 shows the temporal evolution of the drifting speed and mean radius of ball-like flames for two initial perturbations of n = 3.5 and n = 1.5. The ball-like flame radius is calculated based on the volume within the isosurface of c = 0.8. Fig. 14(a) shows that the ball-like flames near the diagonal and near x-axis tend to evolve into the same steady state. Before that, these two ball-like flames drift outwardly maintaining its spherical shape, with periodic expansion and contraction. This is mainly due to the competition between chemical heat release and conductive heat loss to walls. The ball-like flame tends to expand itself during drifting. However, the expansion enhances wall heat loss and in turn reduces the reaction rate and ball-like flame expansion, as shown in Fig. 6. This process continues until the ball-like flame reaches the steady state. For n = 3.5, the mean radius and corresponding drifting velocity approach constant values of r = 1.5 mm and u = 4.5 cm/s) after long time evolution. This value agrees well with the experimental measurement that the propagation speed of ball-like flames is in the range of 4~6 cm/s [19,46]. However, for n = 1.5, the limit value is not observed due to the limited computational domain size. Nevertheless, the drifting speed approaches 4.5 cm/s. Therefore, the evolution of ball-like flames is sensitive to the initial perturbation but the final size and drifting speed seem to be unaffected by the initial perturbation.

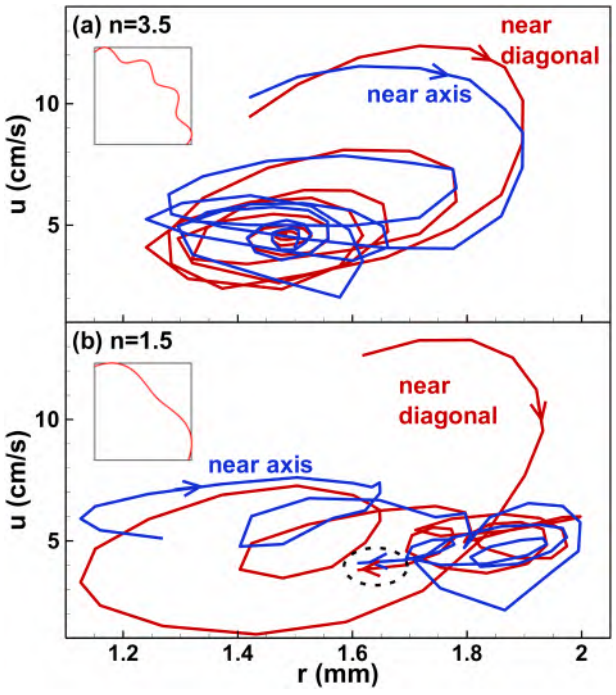

Fig. 14. Evolution of the drifting velocity and mean radius of ball-like flames for ϕ = 0.210. The inserts show initial perturbation on the ignition kernel.

4. Conclusions

We conduct 3D simulations for ultra-lean premixed hydrogen/air flames propagating in an open Hele-Shaw cell with isothermal walls. Detailed chemistry and transport are considered in simulations. By changing the equivalence ratio, different flame regimes reported in previous experiments are observed in our simulations. The flame cell evolution subjected to combined effects of strong diffusional-thermal instability (DTI) and wall heat loss is analyzed.

It is found that the equivalence ratio ϕ has great impact on the propagation of ultra-lean hydrogen/air flames. As ϕ decreases, regimes including two-headed branching, two-headed finger and one-headed finger (ball-like flame), are sequentially observed. To enhance heat release rate affected by curvature and differential diffusion, two-headed and one-headed flame cells tend to reduce the cell size and balance the conductive heat loss in different ways. For two-headed flame cells, heat release rate increases through cell splitting; while for one-headed cells, heat release rate increases by shrinking the ball-like flame size. The integral heat release rate and conductive heat loss are found to correlate with and restrict to each other. Oscillation in total heat release rate, wall heat loss and total flame surface area is observed and the oscillation frequency slightly increases with ϕ. For the first time, it is found that the mutual interaction between the two branches of a two-headed finger flame leads to a large flame segment affected by DLI. Counterintuitively, DLI acts as a stabilizing factor for the two-headed finger flame propagating in a straight path. Synergistic interaction between DLI and DTI can increase the drifting speed of two-headed finger flame. The effect of DLI should be taken into account when modeling the evolution of two-headed finger flame. In addition, the ball-like flames tend to evolve into a steady state with constant size and drifting speed. Though the initial perturbation affects the evolution process, it does not change the final state. Besides, the zigzag motion of ball-like flames before reaching the steady state is caused by cell elongation, weak splitting and subsequent shrinking to ball-like shape.

This work is a first step towards a better understanding of the very interesting flame cell propagation in ultra-lean hydrogen/air mixture

within an open Hele-Shaw cell. In future works, it would be interesting to study the flow/flame ball interaction as well as the effects of radiation, gravity and water vapor condensation on walls.

CRediT authorship contribution statement

Linlin Yang: Writing – review & editing, Writing – original draft, Methodology, Formal analysis, Conceptualization. **Yan Wang:** Writing – review & editing, Formal analysis. **Tianhan Zhang:** Writing – review & editing, Formal analysis. **Xiaolong Gou:** Writing – review & editing, Formal analysis. **Wenjun Kong:** Writing – review & editing, Formal analysis. **Zheng Chen:** Writing – review & editing, Supervision, Methodology, Funding acquisition, Formal analysis, Conceptualization.

Declaration of competing interest

The authors declare that they have no known competing financial interests or personal relationships that could have appeared to influence the work reported in this paper.

Acknowledgements

This work was funded by NSFC, China (No. 52425604) and the Space Application System of China Manned Space Program. We thank Prof. Igor Kirillov and Prof. Mikhail Kuznetsov for helpful discussion and suggestions.

Supplementary materials

Supplementary material associated with this article can be found, in the online version, at doi:10.1016/j.combustflame.2025.114444.

References

[1] J.X. Wen, E.S. Hecht, R. Mevel, Recent advances in combustion science related to hydrogen safety, Prog. Energy Combust. Sci. 107 (2025) 101202.
[2] P.E. Lapenna, L. Berger, F. Creta, H. Pitsch, Hydrogen laminar flames, in: E.-Al. Tingas (Ed.), Hydrog. Future Therm. Engines, Springer International Publishing, Cham, 2023, pp. 93–139.
[3] E.J. Adler, J.R.R.A. Martins, Hydrogen-powered aircraft: fundamental concepts, key technologies, and environmental impacts, Prog. Aerosp. Sci. 141 (2023) 100922.
[4] A.L. Sánchez, F.A. Williams, Recent advances in understanding of flammability characteristics of hydrogen, Prog. Energy Combust. Sci. 41 (2014) 1–55.
[5] B. Lewis, G. Von Elbe, Combustion, Flames and Explosions of Gases, 3rd edition, Academic Press Inc., Orlando, FL, United States, 1987.
[6] A. Onorati, R. Payri, B. Vaglieco, A. Agarwal, C. Bae, G. Bruneaux, M. Canakci, M. Gavaises, M. Günthner, C. Hasse, S. Kokjohn, S.-C. Kong, Y. Moriyoshi, R. Novella, A. Pesyridis, R. Reitz, T. Ryan, R. Wagner, H. Zhao, The role of hydrogen for future internal combustion engines, Int. J. Engine Res. 23 (2022) 529–540.
[7] D. Yu, Z. Chen, Premixed flame ignition: theoretical development, Prog. Energy Combust. Sci. 104 (2024) 101174.
[8] H.D. Ng, J.H.S. Lee, Comments on explosion problems for hydrogen safety, J. Loss Prev. Process Ind. 21 (2008) 136–146.
[9] J.F. Grcar, A new type of steady and stable, laminar, premixed flame in ultra-lean, hydrogen–air combustion, Proc. Combust. Inst. 32 (2009) 1011–1018.
[10] E. Fernández-Tarrazo, A.L. Sánchez, A. Liñán, F.A. Williams, The structure of lean hydrogen-air flame balls, Proc. Combust. Inst. 33 (2011) 1203–1210.
[11] F. Veiga-López, M. Kuznetsov, D. Martínez-Ruiz, E. Fernández-Tarrazo, J. Grune, M. Sánchez-Sanz, Unexpected propagation of ultra-lean hydrogen flames in narrow gaps, Phys. Rev. Lett. 124 (2020) 174501.
[12] J. Yáñez Escanciano, M. Kuznetsov, F. Veiga-López, Characterization of unconventional hydrogen flame propagation in narrow gaps, Phys. Rev. E. 103 (2021) 033101.
[13] P.V. Moskalev, V.P. Denisenko, I.A. Kirillov, Classification and dynamics of ultralean hydrogen–air flames in horizontal cylindrical hele–shaw cells, J. Exp. Theor. Phys. 137 (2023) 104–113.
[14] D. Martínez-Ruiz, F. Veiga-López, M. Sánchez-Sanz, Premixed-flame oscillations in narrow channels, Phys. Rev. Fluids. 4 (2019) 100503.
[15] F. Veiga-López, D. Martínez-Ruiz, M. Kuznetsov, M. Sánchez-Sanz, Thermoacoustic analysis of lean premixed hydrogen flames in narrow vertical channels, Fuel 278 (2020) 118212.
[16] A. Domínguez-González, M.P. Encinar, D. Martínez-Ruiz, Pathway dynamics to double-cell premixed flames in lean hydrogen–air mixtures, Proc. Combust. Inst. 40 (2024) 105496.
[17] A. Domínguez-González, D. Martínez-Ruiz, M. Sánchez-Sanz, Stable circular and double-cell lean hydrogen-air premixed flames in quasi two-dimensional channels, Proc. Combust. Inst. 39 (2023) 1731–1741.
[18] D. Martínez-Ruiz, F. Veiga-López, D. Fernández-Galisteo, V.N. Kurdyumov, M. Sánchez-Sanz, The role of conductive heat losses on the formation of isolated flame cells in Hele-Shaw chambers, Combust. Flame 209 (2019) 187–199.
[19] R. Palomeque-Santiago, A. Domínguez-González, D. Martínez-Ruiz, M. Rubio-Rubio, E. Fernández Tarrazo, M. Sánchez-Sanz, Unveiling the bi-stable character of stealthy hydrogen–air flames, Phys. Fluids 36 (2024) 087137.
[20] Z. Zhou, Y. Shoshin, F.E. Hernández-Pérez, J.A. Van Oijen, L.P.H. De Goey, Effect of pressure on the lean limit flames of H2-CH4-air mixture in tubes, Combust. Flame 183 (2017) 113–125.
[21] P.D. Ronney, Near-limit flame structures at low Lewis number, Combust. Flame 82 (1990) 1–14.
[22] Z. Zhou, Y. Shoshin, F.E. Hernández-Pérez, J.A. Van Oijen, L.P.H. De Goey, Effect of Lewis number on ball-like lean limit flames, Combust. Flame 188 (2018) 77–89.
[23] Y.B. Zeldovich, Theory of Combustion and Detonation of Gases, Academy of Sciences, USSR, 1944.
[24] J. Buckmaster, P. Ronney, Flame-ball drift in the presence of a total diffusive heat flux, Symp. Int. Combust. 27 (1998) 2603–2610.
[25] P.D. Ronney, Understanding combustion processes through microgravity research, Symp. Int. Combust. 27 (1998) 2485–2506.
[26] P.D. Ronney, M.-S. Wu, H.G. Pearlman, K.J. Weiland, Experimental study of flame balls in space: preliminary results from STS-83, AIAA J 36 (1998) 1361–1368.
[27] A. Tsunoda, T. Akiba, H. Nakamura, Y. Morii, T. Tezuka, K. Maruta, Computational study on lean and rich combustion of flame ball, counterflow flame and planar flame: their limits and stoichiometries, Proc. Combust. Inst. 39 (2023) 1937–1944.
[28] R. Fursenko, S. Minaev, H. Nakamura, T. Tezuka, S. Hasegawa, T. Kobayashi, K. Takase, M. Katsuta, M. Kikuchi, K. Maruta, Near-lean limit combustion regimes of low-Lewis-number stretched premixed flames, Combust. Flame 162 (2015) 1712–1718.
[29] T. Okuno, T. Akiba, H. Nakamura, R. Fursenko, S. Minaev, T. Tezuka, S. Hasegawa, M. Kikuchi, K. Maruta, Broken C-shaped extinction curve and near-limit flame behaviors of low Lewis number counterflow flames under microgravity, Combust. Flame 194 (2018) 343–351.
[30] J. Yanez, M. Kuznetsov, F. Veiga-López, On the velocity, size, and temperature of gaseous dendritic flames, Phys. Fluids 34 (2022) 113601.
[31] J. Yanez, L. Kagan, G. Sivashinsky, M. Kuznetsov, Modeling of 2D self-drifting flame-balls in Hele-Shaw cells, Combust. Flame 258 (2023) 113059.
[32] E. Fernández-Tarrazo, R. Gómez-Miguel, M. Sánchez-Sanz, Minimum ignition energy of hydrogen–ammonia blends in air, Fuel 337 (2023) 127128.
[33] L. Esclapez, M. Day, J. Bell, A. Felden, C. Gilet, R. Grout, M.H. De Frahan, E. Motheau, A. Nonaka, L. Owen, B. Perry, J. Rood, N. Wimer, W. Zhang, PeleLMeX: an AMR low mach number reactive flowsimulation code without level sub-cycling, J. Open Source Softw. 8 (2023) 5450.
[34] G.P. Smith, Y. Tao, H. Wang, Foundational Fuel Chemistry Model Version 1.0 (FFCM-1), 2016. http://nanoenergy.stanford.edu/ffcm1.
[35] C. Cuttle, L.C. Morrow, C.W. MacMinn, Compression-driven viscous fingering in a radial Hele-Shaw cell, Phys. Rev. Fluids 8 (2023) 113904.
[36] L. Berger, M. Grinberg, B. Jürgens, P.E. Lapenna, F. Creta, A. Attili, H. Pitsch, Flame fingers and interactions of hydrodynamic and thermodiffusive instabilities in laminar lean hydrogen flames, Proc. Combust. Inst. 39 (2023) 1525–1534.
[37] L. Berger, K. Kleinheinz, A. Attili, H. Pitsch, Characteristic patterns of thermodiffusively unstable premixed lean hydrogen flames, Proc. Combust. Inst. 37 (2019) 1879–1886.
[38] L. Kagan, S. Minaev, G. Sivashinsky, On self-drifting flame balls, Math. Comput. Simul. 65 (2004) 511–520.
[39] T. Akiba, T. Okuno, H. Nakamura, Y. Morii, T. Tezuka, R. Fursenko, S.S. Minaev, M. Kikuchi, K. Maruta, Dynamics of ball-like flames in extremely low-speed counterflow field in near-lean limit low-Lewis number mixture, Proc. Combust. Inst. 38 (2021) 1965–1972.
[40] J.F. MacArt, J.M. Wang, P.P. Popov, J.B. Freund, Detailed simulation of laser-induced ignition, spherical-flame acceleration, and the origins of hydrodynamic instability, Proc. Combust. Inst. 38 (2021) 2341–2349.
[41] A. Patyal, M. Matalon, Nonlinear development of hydrodynamically-unstable flames in three-dimensional laminar flows, Combust. Flame 195 (2018) 128–139.
[42] M. Matalon, C. Cui, J.K. Bechtold, Hydrodynamic theory of premixed flames: effects of stoichiometry, variable transport coefficients and arbitrary reaction orders, J. Fluid Mech. 487 (2003) 179–210.
[43] M. Matalon, Intrinsic Flame Instabilities in Premixed and Nonpremixed Combustion, Annu. Rev. Fluid Mech. 39 (2007) 163–191.
[44] Z. Lu, J. Li, Dynamics of flame rings in a thermally-conductive narrow channel: a numerical experiment, Combust. Theory Model 25 (2021) 1158–1174.
[45] L. Kagan, G. Sivashinsky, Self-fragmentation of nonadiabatic cellular flames, Combust. Flame 108 (1997) 220–226.
[46] A. Elyanov, V. Golub, V. Volodin, P. Alekhnovich, Decay of a hydrogen-air flame front to cup-like cells in a narrow horizontal gap, Process Saf. Environ. Prot. 191 (2024) 1872–1882.